

Depth Estimation from a Single Optical Encoded Image using a Learned Colored-Coded Aperture

Jhon Lopez, Edwin Vargas, *Student Member, IEEE*, Henry Arguello, *Senior Member, IEEE*,

Abstract—Depth estimation from a single image of a conventional camera is a challenging task since depth cues are lost during the acquisition process. State-of-the-art approaches improve the discrimination between different depths by introducing a binary-coded aperture (CA) in the lens aperture that generates different coded blur patterns at different depths. Colored-coded apertures (CCA) can also produce color misalignment in the captured image which can be utilized to estimate disparity. Leveraging advances in deep learning, more recent works have explored the data-driven design of a diffractive optical element (DOE) for encoding depth information through chromatic aberrations. However, compared with binary CA or CCA, DOEs are more expensive to fabricate and require high-precision devices. Different from previous CCA-based approaches that employ few basic colors, in this work we propose a CCA with a greater number of color filters and richer spectral information to optically encode relevant depth information in a single snapshot. Furthermore, we propose to jointly learn the color-coded aperture (CCA) pattern and a convolutional neural network (CNN) to retrieve depth information by using an end-to-end optimization approach. We demonstrate through different experiments on three different data sets that the designed color-encoding has the potential to remove depth ambiguities and provides better depth estimates compared to state-of-the-art approaches. Additionally, we build a low-cost prototype of our CCA using a photographic film and validate the proposed approach in real scenarios.

Index Terms—Depth estimation, End-to-End Optimization, Monocular Vision, Coded-Aperture, Point Spread Function, Depth Cues.

I. INTRODUCTION

WHEN a scene is captured with a conventional camera, the three-dimensional information of the scene is lost and only a two-dimensional representation of the scene is obtained. The retrieval of 3D scene information, particularly the construction of a depth map, has a wide range of applications, including autonomous navigation [1], industrial manufacturing [2], 3D object detection [3], among others. State-of-the-art approaches for depth estimation can be broadly divided into active and passive techniques. Active techniques like LiDAR and structured light imaging typically employ light sources and specialized time-of-flight (ToF) scanning systems [4]. Passive approaches, as the multi-camera system [5] perform triangulation between corresponding points on multiple views of the scene for depth estimation [6]. Stereoscopic and multi-view methods are quite accurate in estimating depth, and have been applied in a wide variety of applications as 3D scene reconstruction [5, 7]. However, there is a continuing need

for compact and low-consumption passive depth estimation technology that is not satisfied with multiple cameras on a single platform. Additionally, while active depth estimation technologies such as LiDAR can provide accurate depth estimation, they require extra components and great energy demand, which can make their usage impractical for certain applications.

On the other hand, monocular vision approaches aim to estimate depth maps from a single image. Traditional approaches of this type are based on Markov Random Fields [8], boosted classifiers [9], or depth from defocus (DFD). DFD approaches recover the depth information from two differently-focused scene images, and it has been studied extensively in computer vision for almost three decades [10–13]. Although the basic theory behind this technique is well known, DFD has found limited use in practice because it requires static scenes, dense surface texture, and images with significant defocus blur [12]. Related approaches, based on defocus, design an optically controlled blur that varies with the scene depth to encode the depth information in a single image using coded apertures (CAs) [14, 15]. For example, Levin et al. [14] design a binary CA to generate optically depth-dependent blur that enables the estimation of an all-in-focus image and a depth map from the acquired coded image. Bando et al. [16] proposed a novel method for acquiring three shifted views of a scene based on optical geometry using a color-coded aperture (CCA). This technique enables the acquisition of multiple views of a scene in the RGB planes of a single exposure, resulting in color misalignment that is depth-dependent. In other words, the captured image provides depth information by analyzing the color shifts induced by the CCA.

On another front, the large amount of available labeled data has led to the rapid growth of deep learning and the development of deep neural network (DNN) architectures with outstanding performance on different areas [17, 18]. For depth estimation, developments in convolutional neural networks (CNNs) have shown that pixel-level depth maps can be recovered from a single image [13, 19]. More recently, a new paradigm, called deep optics [20, 21], exploits deep learning techniques to develop cameras for specific purposes, such as depth estimation [22, 23], spectral imaging [24, 25], light field [26], super-resolution [20], among others. In particular, applications of deep optics for depth estimation include learning a diffractive optical element (DOE) to promote chromatic aberrations as an additional depth-cue to be decoded by a neural network [22, 23, 27]. Although the design and implementation of DOEs have demonstrated high precision in depth estimation, the fabrication of DOEs is expensive,

This work was supported by the Vicerrectoría de Investigación y Extensión of the Universidad Industrial de Santander under the research project 3735 titled "Optical-computer system for acquisition of encoded images for the preservation of privacy and actions recognition in clinical environments"

requires high-precision devices, and can be easily scratched or damaged.

In this work, we propose to design a low-cost and readily manufacturable CCA to optically encode relevant depth information in a single snapshot. While previous research has primarily focused on optical coding with a limited set of basic colors, we propose a CCA with a greater number of color filters and richer spectral information. We leverage the advances of deep learning techniques to jointly learn the optical modulation and the computational decoding algorithm in an end-to-end (E2E) framework. We demonstrate through various computational simulations that our encoding approach outperforms other state-of-the-art encoding alternatives based on CAs, CCAs, or DOEs. Furthermore, we build a prototype of the designed CCA using a photographic film and estimate high-fidelity depth maps demonstrating a cost-effective and practical solution.

II. RELATED WORK

The concept of depth estimation refers to the process of preserving the 3D information of the scene using the 2D information captured by the camera sensors. This task of preserving 3D scene information is currently an area of study in optics and computer vision. Traditional methods for image acquisition and depth estimation can be classified into two sets, active and passive methods.

A. Active Methods

Active methods measure the distance to the objects by measuring the time elapsed from sending pulse signals and their bounce back. These methods are generally based on computing the time of flight of laser, ultrasound, or radio signals of the electromagnetic spectrum to measure and search for objects [28]. Usually, ToF sensors are more suitable for indoor scenarios and short-range ($< 2[m]$) depth sensing, and laser-based scanners (LiDAR) and radars are commonly utilized for 3D measurement outdoors. Key advantages of LiDAR sensors include high resolution, accuracy, high performance in low light, and speed. However, LiDARs are expensive, requiring extensive power resources, thus making them unsuitable for consumer products.

B. Passive Methods

Passive methods exploit characteristics of the captured images, such as the relative size of objects, textures, and blur, among others to estimate depth. In this category of passive methods, there are two main approaches: multi-view depth estimation, such as depth from stereoscopic images, and monocular depth estimation. Stereo imaging is a typical, passive, frequently used depth technique, however, it can present ambiguity in texture information, so the only solution to this problem is to use more cameras [29], which increases the cost, space of these systems, and calibration. An alternative approach to these drawbacks is to use a single-camera (monocular) system, which is fundamentally different from depth estimation from stereo pairs because triangulation is no

longer possible. In a monocular setting, contextual information is required, e.g., texture variation, occlusions, scene context [30], but mainly over the years, defocus-blur has been explored as a depth cue.

C. Coded Defocus Blur

Depth from defocus (DFD) can be achieved by exploiting the fact that optical blur varies with the scene depth. Specifically, DFD approaches recover depth information from two differently-focused scene images, and it has been studied extensively in computer vision for almost three decades [10–13]. Nayar et al. [31] proposed to use a prism between a lens and an image sensor to capture two photos with varying focus distances from the same viewpoint. The authors in [32] employed a multi-focus camera to collect three photos with varying focus distances, and introduced a coded aperture to estimate the depth map and a blur-free image of the scene using an inverse filter [33]. However, multiple captures with coded apertures are only feasible for static scenes.

To overcome this limitation, various approaches harness the advantages of CCAs [16, 34–36]. Optically, CCAs can induce different degrees of blur in each RGB channel of the captured image generating color misalignment along channels. Therefore, depth estimation can be inferred from the disparity observed across the sensor channels eliminating the need for multiple captures. More precisely, the use of CCA for depth estimation was first proposed in 1993 in [34], by using red and green filters jointly with an algorithm based on the color gradient, to estimate the disparity. Bando et al. [16] also explored a CCA by dividing the aperture into three regions through which light can only pass in one of the RGB color bands, acquiring three displaced views of a scene in the RGB planes. Bando et al. [16] proposed to include the blue color and divide the CCA into three regions in order to acquire three displaced views of a scene in the RGB planes. Since [34] and [16] have low light efficiency, a high transmittance CCA has been proposed by using the CMYK color space [36]. Fig.2 shows state-of-the-art CCAs for depth estimation.

D. Deep Optics

Optics and algorithm design are both involved in computational imaging systems. Deep optics treats the entire system as one neural network and develops an end-to-end optimization framework, rather than optimizing these two components separately and sequentially. The first layer of the network, in particular, corresponds to physical optical elements, while all subsequent layers represent the computational algorithm. All the parameters are learned over a large dataset using a task-specific loss. This technique has been successfully applied in specific tasks such as spectral imaging [25, 37], depth estimation [22, 23, 38], light field [26], super-resolution imaging [20] and in compound task as spectral-depth reconstruction [24].

III. PROPOSED METHOD

This work considers a monocular system that encodes depth information by leveraging a CCA, as shown in Fig. 1. In

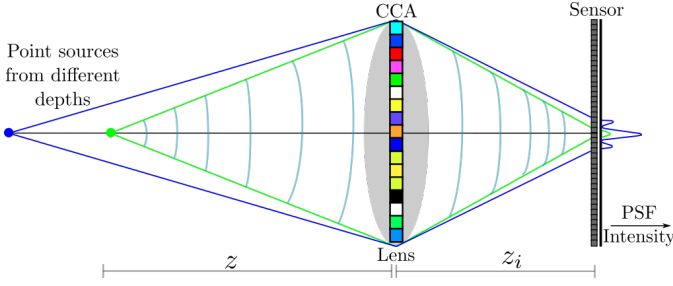


Fig. 1. Optical propagation model of point sources through a color-coded aperture in front of a thin lens.

contrast with state-of-the-art CCA with few basic colors as shown in Fig. 2, we propose to design CCA with a greater number of color filters and richer spectral information. As we mentioned before, the performance of this system mainly depends on the CCA and the recovery algorithm used to decode the depth information. Therefore, we propose to jointly learn the CCA of the optical encoder and a neural network working as a decoder in an end-to-end manner. Fig. 3 presents our proposed solution consisting of two main components: 1) a differentiable optical layer, whose trainable parameters are the color-coded aperture values, and 2) a U-Net network [17] for depth estimation. During training, the optical layer is fed with a given all-in-focus spectral image and its corresponding ground-truth depth map and it generates the simulated encoded sensor RGB image. The encoded image is then fed to the U-Net network, which produces the estimated depth. The loss between the estimated depth map and the ground truth depth is calculated to optimize the optical layer and network weights via back-propagation [39]. In the next subsection, we present in more detail the forward model of the proposed system, including the parametrization of the CCA.

A. Image Formation Model

We create a camera model with a single convex thin lens with a focal length f at distance z_i from the sensor and a CCA in the lens as shown in Fig. 1. Most of the real-world scenes contain objects at various depths that are imaged with different PSFs. To simulate the PSF for every depth z , consider a point emitter with wavelength λ centered on the optical axis and located a distance z away from the lens center.

By propagating this point, the electric field of the spherical wave arriving at the lens is given by the Fresnel approximation¹ as:

$$U_{\text{in}}^{\lambda,z}(x,y) = \exp\left[i\frac{2\pi}{\lambda}\frac{x^2+y^2}{z}\right]. \quad (1)$$

The wavefront then propagates through the lens with the lens phase delay being, $t(x,y)$:

$$t^\lambda(x,y) = \exp\left[-i\frac{k}{2f}(x^2+y^2)\right], \quad (2)$$

where $k = 2\pi/\lambda$ is the wavenumber. Because a lens has a finite aperture size, we insert an amplitude function $A(x,y)$

¹It assumes that the wavelength λ is significantly smaller than the travel distance z : $\lambda \ll z$.

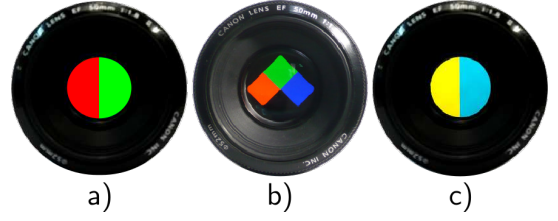


Fig. 2. State-of-the-art color-coded apertures. a) [34], b) [16] and c) [36].

that blocks all light outside the open aperture. We also add the function $T(x,y,\lambda)$, which represents the CCA separated by a distance z_t from the lens.² Assuming that the CCA wavelength response remains approximately constant over a spatial region of size $\Delta_m \times \Delta_m$ and wavelength interval Δ_d , the CCA can be modeled using a rectangular function as follows:

$$T(x,y,\lambda) = \sum_{i,j,\ell} W_{i,j,\ell} \text{rect}\left(\frac{x}{\Delta_m} - i, \frac{y}{\Delta_m} - j, \frac{\lambda}{\Delta_d} - \ell\right), \quad (3)$$

where $W_{i,j,\ell} \in [0,1]$ represents the discretized light response of the colored-coded aperture in the (i,j) -th position, and ℓ -th spectral band of the discretized voxels [37, 40]. The above CCA model is generally applicable, where a square CCA with a filter matrix $N \times N$ and L spectral bands results in N^2L parameters $W_{i,j,\ell}$. However, practical constraints, such as manufacturing limitations [41], restrict the ability to customize filter spectral responses arbitrarily. In line with Henry et al. [37], the colors of the proposed CCA design are obtained by forming linear combinations of 4 primary colors (green, red, blue, and cyan). This approach yields filter colors:

$$C^r(\lambda) = \sum_{\ell=0}^{L-1} \alpha_\ell^r \text{rect}\left(\frac{\lambda}{\Delta_d} - \ell\right), \quad (4)$$

where α_ℓ^r represents the discrete spectral response of the r -th primary filter, which is predetermined based on available materials or chemical components. Using (4), the CCA for our optical configuration can be finally expressed as:

$$T(x,y,\lambda) = \sum_{i,j} \sum_{r=0}^{R-1} \sum_{\ell=0}^{L-1} w_{i,j,r} \alpha_\ell^r \text{rect}\left(\frac{x}{\Delta_m} - i, \frac{y}{\Delta_m} - j, \frac{\lambda}{\Delta_d} - \ell\right), \quad (5)$$

where R is the number of primary filters, and $w_{i,j,r} \in [0,1]$ represents the CCA weights for the i -th row, j -th column, and r -th primary filter. The electric field immediately after the lens and CCA is:

$$U_{\text{out}}^{\lambda,z}(x,y) = A(x,y)T(x,y,\lambda)t^\lambda(x,y)U_{\text{in}}^{\lambda,z}(x,y). \quad (6)$$

We propagate $U_{\text{out}}^{\lambda,z}(x,y)$ a distance z_i to the sensor using the exact transfer function [42]

$$H_{z_i}(f_x, f_y) = \exp\left[ikz_i\sqrt{1 - (\lambda f_x)^2 - (\lambda f_y)^2}\right], \quad (7)$$

²The proposed method assumes the CCA is attached to the lens, i.e. $z_t \approx 0$.

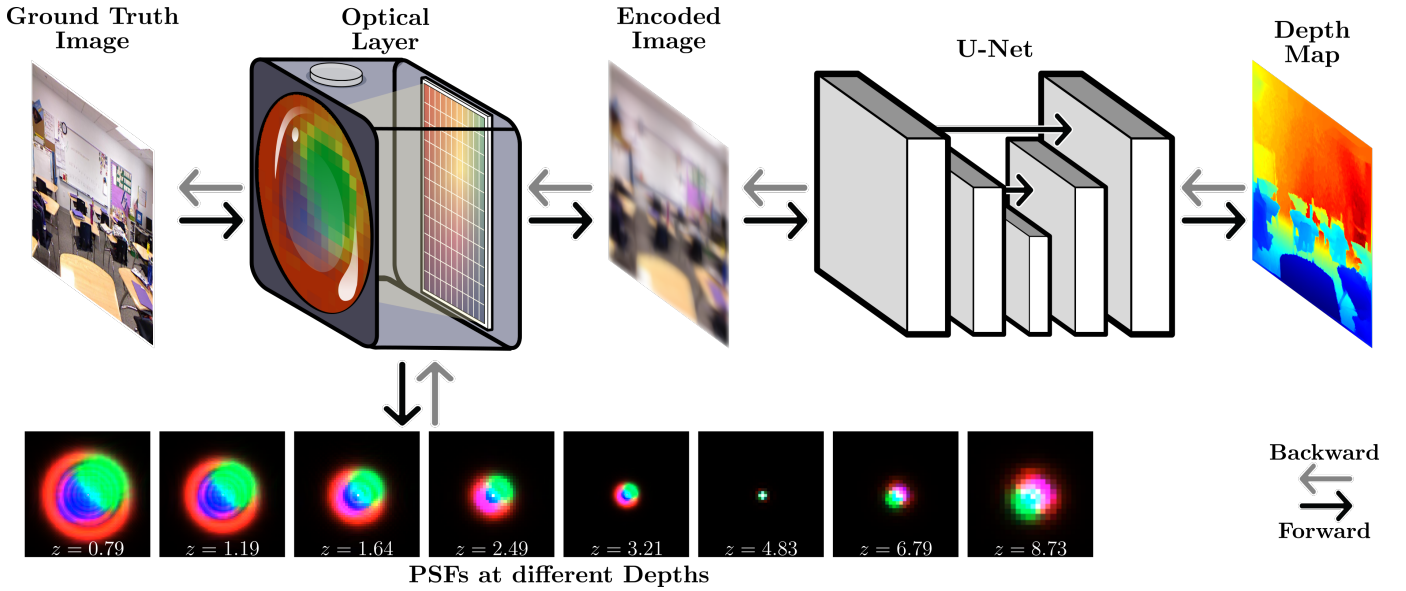


Fig. 3. Our proposed architecture consists of two parts. In the optical layer, digital modeling of depth-dependent PSFs is performed from an optimized color aperture code, thus obtaining a depth-encoded image. In the reconstruction network, we use a U-Net-based network for depth estimation from the coded image. The optical layer and reconstruction network parameters are optimized based on the defined loss between the estimated depth and the reference depth map.

to finally obtain the field in the sensor

$$U_{\text{sen}}^{\lambda,z}(x', y') = \mathcal{F}^{-1} \left\{ \mathcal{F} \left\{ U_{\text{out}}^{\lambda,z}(x, y) \right\} \cdot H_{z_i}(f_x, f_y) \right\}, \quad (8)$$

where (f_x, f_y) are spatial frequencies and \mathcal{F} denotes the 2D Fourier transform. Since the sensor acquires light intensity, the PSF for each depth and wavelength is obtained using the magnitude-squared of (8):

$$\text{PSF}_{\lambda,z}(x', y') = |U_{\text{sen}}^{\lambda,z}(x', y')|^2. \quad (9)$$

B. Depth-Dependent Image Formation Model

The simulated PSFs are employed to approximate the captured image by an RGB sensor of a given 3D scene using a layered representation that models the scene as a set of surfaces on discrete depth planes [43]. This allows the precomputation of a fixed number of PSFs corresponding to each depth plane. We make few modifications here to suit our datasets consisting of pairs of all-in-focus spectral images and their discretized depth maps. Considering an all-in-focus spectral image \mathbf{I} , and a set of $j = 1 \dots J$ discrete depth layers, and corresponding occlusion masks \mathbf{M}_j , the encoded spectral image at wavelength λ is:

$$\hat{\mathbf{I}}_{\lambda} = \sum_{j=1}^J (\mathbf{I}_{\lambda} * \text{PSF}_{\lambda,j}) \odot \mathbf{M}_j, \quad (10)$$

where $*$ denotes 2D convolution and \odot denotes element-wise multiplication. The cumulative occlusion masks \mathbf{M}_j are alpha masks that modulate how much light from each layer is captured by the sensor at each pixel, to ensure smooth transitions between depths[22]. The alpha masks are generated by blurring binary depth masks \mathbf{A}_j (indicating presence (1) or

absence (0) of objects at the j -th depth layer) from current and preceding layers:

$$\begin{aligned} \mathbf{M}'_j &= (1 - \mathbf{M}_{j+1}) (\mathbf{A}_j * \text{PSF}_j), \text{ for } j < J \\ \mathbf{M}'_J &= \mathbf{A}_J * \text{PSF}_J \end{aligned} \quad (11)$$

Here, layer J is the layer closest to the camera that is not occluded by any additional layers, so \mathbf{M}'_J simply consists of the regions of the depth map that fall into layer \mathbf{A}_J , blurred by PSF_J [22]. Each layer behind J is occluded by the layers in front of it. Finally, \mathbf{M}'_j are normalized to \mathbf{M}_j such that the sum of occlusion mask weights at each pixel location sums to 1. Finally, the RGB channels of the captured image can be modeled as

$$\ddot{\mathbf{I}}_c = \int \hat{\mathbf{I}}_{\lambda} \mathcal{R}_c(\lambda) d\lambda, \text{ for } c = 1, 2, 3. \quad (12)$$

where $\mathcal{R}_c(\lambda)$ represents the spectral response of the c -th channel.

C. Depth Reconstruction Network

We use an encoder-decoder scheme based on convolutional neural networks, where the encoder is in charge of simulating the optical process of image acquisition, and the decoder extracts the depth information present in the encoded images. We adopt the U-Net architecture for the decoding process since it is widely used for pixel-level prediction, and it is adequate for depth estimation. This scheme is illustrated in Fig. 3.

1) *Training Loss Function*: To optimize all the parameters of our model, the following cost functions were employed:

$$\mathcal{L} = \alpha \mathcal{L}_g + \mu \mathcal{L}_n + \sigma \mathcal{L}_s \quad (13)$$

where \mathcal{L} is the total loss and $\alpha, \mu, \sigma \in \mathbb{R}$ are weighting coefficients for each loss. The description of each term of the total loss function is as follows:

- **Gradient loss** \mathcal{L}_g : In an image, it is common to have different objects at different depths, which can generate sharp transitions in the estimated depth map. To account for this, we use an edge-dependent loss function defined given by:

$$\mathcal{L}_g = \frac{1}{M} \sum_{i,j} \|\nabla Y_{i,j} - \nabla \tilde{Y}_{i,j}\|^2 \quad (14)$$

where ∇ is the 2-D Sobel edge detection operator [44], Y and \tilde{Y} represent the original and estimated depth maps, respectively, and M is the total number of depth pixels.

- **Normal Loss** \mathcal{L}_n : In natural scenes, large objects have a greater impact on neural network depth estimation than small objects. This is because the network predicts depth by comparing it to surrounding object depths. To address this, we use a loss function, \mathcal{L}_n , which assesses the accuracy between the surface normal of the estimated depth map and the ground truth:

$$\mathcal{L}_n = 1 - \frac{\langle n, \tilde{n} \rangle}{\max(\|n\|_2, \|\tilde{n}\|_2)}, \quad (15)$$

where $n = [\nabla Y, 1]^T$ and $\tilde{n} = [\nabla \tilde{Y}, 1]^T$.

- **Smoothness** \mathcal{L}_s : Because outliers may exist in some depth map estimates [45], we chose a cost function that globally evaluates the estimated depth maps.

$$\mathcal{L}_s = \begin{cases} 0.5d^2 & \text{if } |d| < 1 \\ |d| - 0.5 & \text{otherwise,} \end{cases} \quad (16)$$

where $d = Y - \tilde{Y}$. \mathcal{L}_s is a robust version of the ℓ_1 norm that is more sensitive to outliers than the ℓ_2 norm [46].

2) *CCA Constraint Design*: To design the CCA using the end-to-end approach, we use a composed constraint to ensure that the designed CCA is manufacturable. This constraint uses the CLIP function [47] to restrict the values within the interval $[0, 1]$ and normalization over primary filter colors coefficient (w in (5)) to avoid the CCA amplifying the incident light in the lens. The constraint can be described as:

$$w_{i,j,r} = \text{CLIP} \left(\frac{w_{i,j,r}}{\sum_{r=0}^{R-1} w_{i,j,r}} \right), \quad (17)$$

where R is the number of color filters in the CCA.

3) *Training details*: Given the forward model and the loss function, the chain rule can derive the back-propagation error. In our system, back-propagation is obtained using automatic differentiation implemented in the PyTorch framework [48]. During the training, we use the Adam optimizer with parameters $\beta_1 = 0.99$ and $\beta_2 = 0.999$. Empirically, we found that using different learning rates for the optical layer and depth reconstruction network (U-Net) improves the performance. We used a training minibatch size of 32. The training and testing were performed on a NVIDIA GeForce RTX 3090 GPU.

IV. SIMULATIONS AND RESULTS

In this section, we evaluate the proposed approach in simulation on different datasets and provide comparisons with respect to other depth estimation methods. Furthermore, we performed ablation studies, which led us to discriminate the contribution of the principal components of our method.

A. Datasets

To perform the computational simulations, we need datasets that contain color or spectral information, therefore, the following datasets containing 31 spectral bands equally spaced from 400 to 700 nanometers were used:

- **NYU-S**: Since a large dataset with spectral and continuous depth information is not yet available, to prove the hypothesis of our approach, we generate fake spectral images with 31 bands from the RGB images in the NYU dataset [49] by using the CNN proposed by Yuzhi et al. [50], see Fig. 4. The NYU-S dataset contains 1450 fake spectral images with their corresponding depth maps. Additionally, we used the default training/testing splits provided in [49] and performed random cropping with window sizes of 256×256 to augment the training set.

- **Baek**: Real spectral-depth dataset published in Baek et al. [24] (see Fig. 4). This dataset contains 18 spectral images with 31 bands and their corresponding depth map. During training, 13 images were used and 5 images were used for testing. To increase the variability of the data during training, a random cropping with window sizes of 512×512 was conducted.

- **Custom**: Due to the limited amount of spectral-depth data from the dataset mentioned above, we decided to acquire our own dataset, which contains 63 spectral images with their corresponding depth map, see Fig. 4. The acquisition of the spectral images was carried out by illuminating the scene with a tunable light source ³ (TLS), which offers wavelengths in the range of 300 – 1800 nm. We used wavelengths between 400 – 700 nm with intervals of 10 nm. The depth maps vary in a range of 0.4 – 1.6 m, estimated using the structured light (SL) setup shown in Fig.5 and the phase unwrapping via graph cuts algorithm [51].

B. Evaluation

Following previous works [22, 52], we adopt the following evaluation metrics to quantitatively assess the performance of our depth prediction model. Specifically, we use:

- Mean Absolute Error (MAE): $\frac{1}{N} \sum_{i=1}^N |y_i - \tilde{y}_i|$
- Mean Relative Error (REL): $\frac{1}{N} \sum_i \frac{|y_i - \tilde{y}_i|}{\tilde{y}_i}$
- Mean Log₁₀ Error (Log₁₀): $\frac{1}{N} \sum_i |\log_{10}(y_i) - \log_{10}(\tilde{y}_i)|$
- Root Mean Squared (RMSE): $\sqrt{\frac{1}{N} \sum_i |y_i - \tilde{y}_i|^2}$
- Thresholded Accuracy (δ_j): $\frac{1}{N} \sum_i \max\left(\frac{\tilde{y}_i}{y_i}, \frac{y_i}{\tilde{y}_i}\right) < 1.25^j$, where y_i and \tilde{y}_i are ground-truth and estimated depth map respectively, N is the total depth map pixels and $j = \{1, 2, 3\}$. Smaller values on REL, Log₁₀, and RMS error are better, and higher values on δ_j threshold are better.

C. CCA design

We compared the proposed depth estimation approach with several baseline approaches based on CAs and CCAs to demonstrate the advantages of the proposed CCA design. The baselines were trained using the NYU-S dataset and are as follows:

³<https://www.newport.com/p/TLS130B-300X>

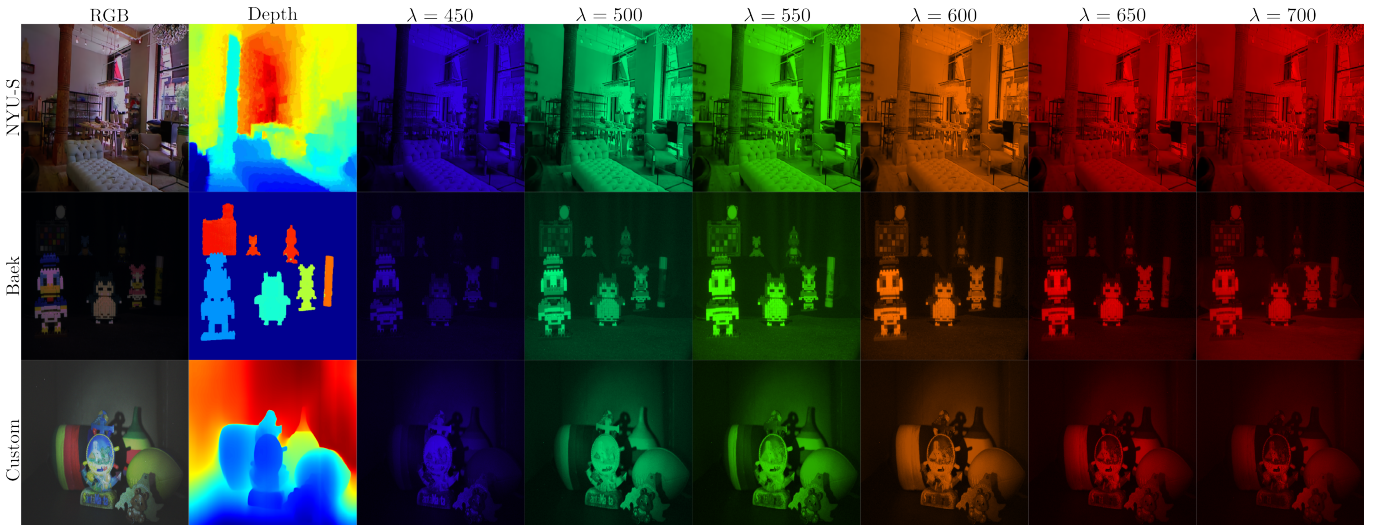


Fig. 4. RGB image, depth map, and some spectral bands of scenes from the three datasets employed for validation. The RGB image shows the overall appearance of the scene, while the depth map provides information about the distance of objects from the camera. In this work, the intensities of different spectral bands are employed to codify depth information by leveraging a CCA.

- **Vanilla:** Training of the vanilla U-Net neural network for depth estimation, without the addition of optical layers and a learning rate of $5e^{-4}$.
- **Fixed-BCA:** In this set-up, we fixed a random binary coded aperture (BCA), which filters the light entirely in certain regions of the image plane, and only optimizes a U-Net for depth estimation.
- **Levin-BCA [14]** This baseline is similar to the previous one, with the difference that the BCA is the code optimized with genetic algorithms by Levin et al. [14] for depth estimation.
- **Learned-BCA:** This baseline uses the proposed end-to-end scheme to obtain an optimal BCA for monocular depth estimation, using a learning rate of 1^{-3} for the optical layer and a learning rate of 5^{-4} for the neuronal network. We use the optimization scheme proposed by Bacca et al. [40] to obtain binary values.
- **Bando-CCA [16]:** In this baseline, the RGB-coded aperture proposed by Bando et al. [16] is used, and optimize the U-Net parameters to extract the depth map from the encoded image, with a learning rate of $5e^{-4}$.
- **Fixed-CCA:** In this set-up, we fixed a random CCA and trained only U-Net parameters with a learning rate of 5^{-4} .
- **Learned-CCA:** For our proposed approach, the learning rates for the optical layer and U-Net were $5e^{-2}$ and $5e^{-4}$, respectively.

TABLE I
QUANTITATIVE RESULTS OF ABLATION STUDIES ON THE NYU-S DATASET. THE BEST RESULTS ARE IN BOLD, AND THE SECOND-BEST ARE UNDERLINED.

Exp	RMS↓	REL↓	Log ₁₀ ↓	δ_1 ↑	δ_2 ↑	δ_3 ↑
Vanilla	0.848	0.276	0.107	0.619	0.856	0.942
Fixed-BCA	0.226	0.055	0.024	0.975	0.996	0.994
Levin-BCA:	0.208	0.053	0.022	0.979	0.998	0.998
Learned-BCA	<u>0.196</u>	<u>0.051</u>	<u>0.021</u>	<u>0.979</u>	<u>0.996</u>	<u>0.998</u>
Bando-CCA	0.224	0.067	0.028	0.968	0.995	0.996
Fixed-CCA	0.214	0.060	0.025	0.968	0.996	0.997
Learned-CCA	0.147	0.039	0.016	0.993	0.998	0.999

Table I presents the quantitative results of the different baselines compared with the proposed approach. The *Vanilla* approach demonstrates that using only the U-Net architecture without incorporating optical coding is inadequate for depth estimation, as all other experiments using a coded aperture achieve superior performance. In particular, the *Levin-BCA* and *Learned-BCA* baselines reveal that using an optimized coded aperture contributes to more accurate depth estimation compared to the *Fixed-BCA* baseline. Comparing the colored approach *Bando-CCA* with the naive *Fixed-CCA* approach demonstrates that using more colors improves depth

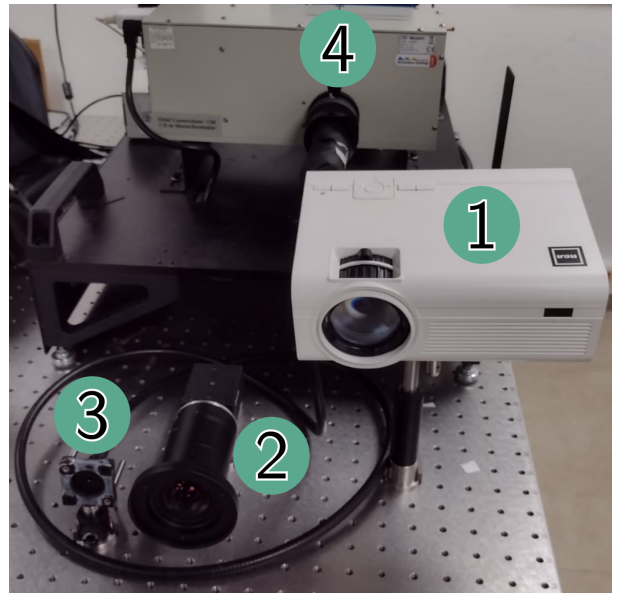


Fig. 5. Optical system used to acquire our own spectral-depth dataset using spectral scanning and structured light. The light projector (1) emits a collimated beam of structured light patterns that is captured by the camera (2). The tunable light source (4) emits selective wavelengths to travel through an optical fiber (3) to illuminate the scene which is also captured with camera (2).

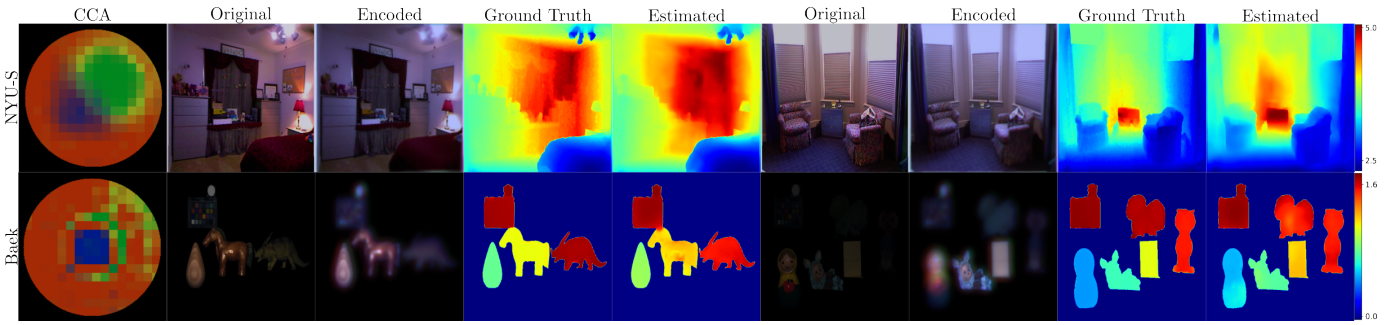


Fig. 6. Visual results on the NYU-S and Baek datasets, along the learned color-coded aperture. The reconstructed depth maps closely match the ground truth depth maps in both datasets.

TABLE II

QUANTITATIVE COMPARISON OF THE PROPOSED APPROACH WITH STATE-OF-THE-ART MODELS ON THE NYU-DEPTH TEST SET. THE BEST RESULTS ARE IN BOLD, AND THE SECOND-BEST ARE UNDERLINED.

Model	REL↓	RMS↓	Log ₁₀ ↓	δ_1 ↑	δ_2 ↑	δ_3 ↑
DORN [53]	0.115	0.509	0.051	0.828	0.965	0.992
MS-CRF [54]	0.121	0.586	0.052	0.811	0.954	0.987
2S-CNN [55]	0.152	0.611	0.064	0.789	0.955	0.988
Make3D [56]	0.349	1.214	-	0.447	0.745	0.897
UP-CNN [57]	0.127	0.573	0.055	0.811	0.953	0.988
DPT [52]	0.110	0.357	0.045	0.904	0.988	<u>0.998</u>
VNL [58]	0.108	0.416	0.048	0.875	0.976	0.994
BTS [59]	0.110	0.392	0.047	0.885	0.978	0.995
LapDepth [60]	0.105	0.384	0.045	0.895	0.983	0.996
AdaBins [61]	0.103	0.364	0.044	0.903	0.984	0.997
Chang et al. [22]	0.087	0.432	0.052	0.930	0.990	<u>0.998</u>
Wu et al. [23]	0.093	0.382	0.050	0.932	0.989	0.997
Learned-BCA	0.051	0.196	0.021	0.979	0.996	0.998
Learned-CCA	0.039	0.147	0.016	0.993	0.998	0.999

estimation. However, *Bando-CCA* and *Fixed-CCA* baselines also show that the use of CCA without any optimization criteria produces suboptimal results, as is evident from the superior performance obtained in the *Levin-CA* and *Learned-BCA* experiments. The proposed approach achieves the best performance in all metrics highlighting the advantage of the learned color codification for high-throughput depth estimation.

D. Monocular depth estimation

Once validated our proposed CCA-based depth estimation approach, we compare our method with state-of-the-art monocular approaches [52–61] that employ all-in-focus RGB images (without optimized optical coding). We also compare our method with approaches that perform end-to-end optimization of DOEs that promote chromatic aberrations as depth cues [22–24]. Additionally, we include the results of the proposed approach but the coded aperture is constrained to be binary (*Learned-BCA*). The quantitative results performed in the default NYU-S test set are compiled in Table II. Our colored-controlled-defocus approach achieves superior accuracy in all metrics, demonstrating that coding across the visible spectrum contributes to improved depth estimation using a simple decoder such as the U-Net. Furthermore, the experimental results show that optimizing BCA using the proposed approach achieves comparable performance to state-of-the-art DOEs. The top of Fig. 6 shows the learned

TABLE III

QUANTITATIVE RESULTS OVER TEST-SET IN THE BAEK DATASET.

Method	Chang et al. [22]	Wu et al. [23]	Baek et al. [24]	Ours
RMSE	0.45	0.31	0.20	0.18
MAE	0.25	0.19	0.12	0.12

CCA, examples of encoded images, and estimated depth maps for NYU-S datasets. These qualitative results show that the estimated depth maps preserve high fidelity to the ground truth.

Performance on Baek dataset Finally, we learned our encoder-decoder model using Baek dataset. Visual results of the learned CCA, encoded image, and recovered depth maps are shown at the bottom of Fig. 6, demonstrating also accurate depth estimation. Since the Baek dataset contains few images with considerable dark areas, there is a noticeable difference in the obtained CCA in this experiment compared to the CCA learned with the NYU-S dataset. Additionally, Table III presents quantitative results (adapted from [24]) comparing our method with state-of-the-art approaches that learn DOEs [22–24]. They show that our method achieves similar or higher results with the advantage of using an optical element that can be implemented with a low-cost photographic film as demonstrated in the following section.

V. EXPERIMENTS ON REAL HARDWARE

After rigorously validating our method with state-of-the-art datasets in simulation, we validate our proposed approach with real captures. First, the proposed model is learned using our *Custom* dataset. Figure 7 shows optimized CCA, encoded images, and corresponding estimated depth maps. The depth maps largely match the actual values, demonstrating the robustness of our method. Note that the learned CAs using NYU-S and *Custom* data have similar structures; confirming that the interpolated spectral images in NYU-S yield close results to spectral images acquired with a real spectral imager.

Second, we build a test-bed prototype shown in Fig. 8. This system incorporates two Thorlabs Achromatic Doublets lenses⁴ with focal lengths of 50 mm and 100 mm. These lenses are carefully arranged to form a composite lens configuration, with

⁴https://www.thorlabs.com/newgrouppage9.cfm?objectgroup_id=2696

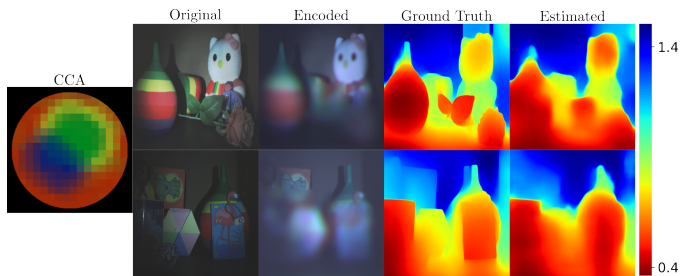


Fig. 7. Visual results using the Custom dataset, with the optimized color-coded aperture. The reconstructed depth maps closely match the ground truth depth maps.

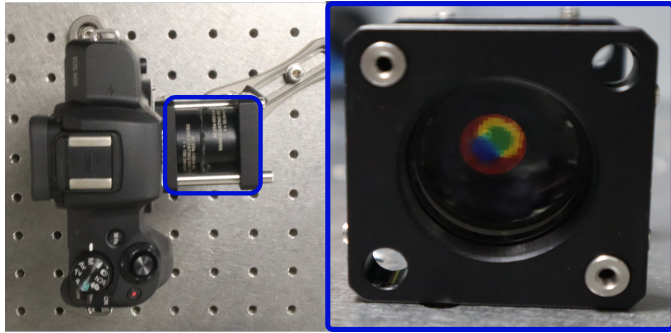


Fig. 8. Testbed implementation of the proposed optical system along the optimized CCA implemented with a color photographic film.

our optimized CCA positioned at the center. This configuration aims to closely approximate the simulated model, as depicted in Fig. 1. This system is adapted to a Canon camera (EOS M50) with a CMOS sensor of 24.1 megapixels (see Fig. 8). To fabricate the optimized CCA, we use a color FUJICHROME Velvia 50 transparency film [62] (35 mm, 36 exposures) and the printing process used in [37]. The printed CCA is shown in the inset of Fig. 8. Once the system is implemented, the performance of the proposed method may be affected by mismatch and fabrication errors of the CCA. Therefore, we capture the real PSFs (see Fig 9) by using a white light point source and calibrating the simulated PSFs with the captured PSFs. Then, with the calibrated PSFs, we fine-tune the U-Net depth estimation network for 100 epochs, a learning rate of $3e - 5$, and our *Custom* dataset.

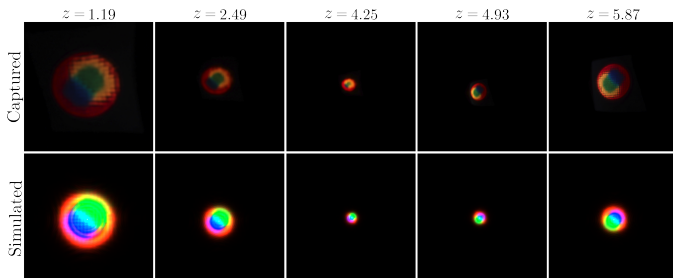


Fig. 9. Real and simulated PSFs at different depths in meters.

We also capture an all-in-focus version of the same scene using an identical camera setup without employing any optical coding and estimate a depth map utilizing a U-Net trained

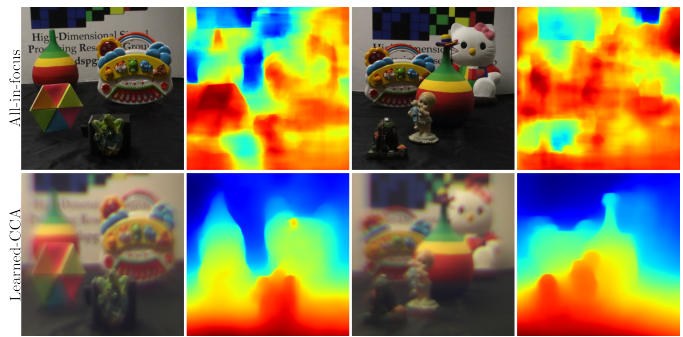


Fig. 10. Real depth map predictions from our proposed spectral encoded images and all-in focus images.

using the NYU dataset. The real captured images and depth map estimates are illustrated in Fig. 10. These results, demonstrate that our proposed approach (*Learned-CCA*) exhibits remarkable robustness in accurately estimating depth maps within indoor scenes, in contrast to the approach without any coding methodology. Furthermore, the results of this experiment demonstrate the feasibility of implementing the proposed spectral codification by leveraging color photographic films.

VI. CONCLUSIONS

In this work, we design a color-coded aperture (CCA) using an end-to-end optimization approach for encoding the depth information using a monocular system. Compared with CCA-based approaches that employ few colors for encoding depth information, the proposed approach demonstrates that using more color filters with rich spectral information significantly improves depth estimation. On the other hand, our approach ratifies, that the data-driven design of specific-purpose optical elements using the E2E technique, allows better depth encoding, compared to CCA used without any data constraint. We built a prototype camera using the optimized CCA and recover high-fidelity depth maps using a fine-tuned neural network validating our proposed approach in real scenarios. The proposed color codification can be fabricated using a low-cost photographic film and established film development, highlighting the additional economic benefit of the proposed codification compared with high-cost DOEs.

REFERENCES

- [1] S. Royo and M. Ballesta-Garcia, "An overview of lidar imaging systems for autonomous vehicles," *Applied sciences*, vol. 9, no. 19, p. 4093, 2019.
- [2] Z. Ni, Z. Shen, C. Guo, G. Xiong, T. Nyberg, X. Shang, S. Li, and Y. Wang, "The application of the depth camera in the social manufacturing: a review," in *2016 IEEE International Conference on Service Operations and Logistics, and Informatics (SOLI)*. IEEE, 2016, pp. 66–70.
- [3] A. Shrivastava and A. Gupta, "Building part-based object detectors via 3d geometry," in *Proceedings of the IEEE International Conference on Computer Vision*, 2013, pp. 1745–1752.

- [4] Z. Wang, “Review of real-time three-dimensional shape measurement techniques,” *Measurement*, vol. 156, p. 107624, 2020.
- [5] Y. Liu, X. Cao, Q. Dai, and W. Xu, “Continuous depth estimation for multi-view stereo,” in *2009 IEEE Conference on Computer Vision and Pattern Recognition*. IEEE, 2009, pp. 2121–2128.
- [6] A. M. Andrew, “Multiple view geometry in computer vision,” *Kybernetes*, 2001.
- [7] C. Hane, C. Zach, A. Cohen, R. Angst, and M. Pollefeys, “Joint 3d scene reconstruction and class segmentation,” in *Proceedings of the IEEE Conference on Computer Vision and Pattern Recognition*, 2013, pp. 97–104.
- [8] A. Saxena, M. Sun, and A. Y. Ng, “Make3d: Learning 3d scene structure from a single still image,” *IEEE transactions on pattern analysis and machine intelligence*, vol. 31, no. 5, pp. 824–840, 2008.
- [9] L. Ladicky, J. Shi, and M. Pollefeys, “Pulling things out of perspective,” in *Proceedings of the IEEE conference on computer vision and pattern recognition*, 2014, pp. 89–96.
- [10] P. Favaro, “Recovering thin structures via nonlocal-means regularization with application to depth from defocus,” in *2010 IEEE Computer Society Conference on Computer Vision and Pattern Recognition*. IEEE, 2010, pp. 1133–1140.
- [11] E. Alexander, Q. Guo, S. Koppal, S. Gortler, and T. Zickler, “Focal flow: Measuring distance and velocity with defocus and differential motion,” in *European conference on computer vision*. Springer, 2016, pp. 667–682.
- [12] H. Tang, S. Cohen, B. Price, S. Schiller, and K. N. Kutulakos, “Depth from defocus in the wild,” in *Proceedings of the IEEE Conference on Computer Vision and Pattern Recognition*, 2017, pp. 2740–2748.
- [13] M. Carvalho, B. Le Saux, P. Trouvé-Peloux, A. Almansa, and F. Champagnat, “Deep depth from defocus: how can defocus blur improve 3d estimation using dense neural networks?” in *Proceedings of the European Conference on Computer Vision (ECCV) Workshops*, 2018, pp. 0–0.
- [14] A. Levin, R. Fergus, F. Durand, and W. T. Freeman, “Image and depth from a conventional camera with a coded aperture,” *ACM transactions on graphics (TOG)*, vol. 26, no. 3, pp. 70–es, 2007.
- [15] P. A. Shedligeri, S. Mohan, and K. Mitra, “Data driven coded aperture design for depth recovery,” in *2017 IEEE International Conference on Image Processing (ICIP)*. IEEE, 2017, pp. 56–60.
- [16] Y. Bando, B.-Y. Chen, and T. Nishita, “Extracting depth and matte using a color-filtered aperture,” in *ACM SIGGRAPH Asia 2008 papers*, 2008, pp. 1–9.
- [17] O. Ronneberger, P. Fischer, and T. Brox, “U-net: Convolutional networks for biomedical image segmentation,” in *International Conference on Medical image computing and computer-assisted intervention*. Springer, 2015, pp. 234–241.
- [18] K. Wang, D. Zhang, Y. Li, R. Zhang, and L. Lin, “Cost-effective active learning for deep image classification,” *IEEE Transactions on Circuits and Systems for Video Technology*, vol. 27, no. 12, pp. 2591–2600, 2016.
- [19] C. Zhao, Q. Sun, C. Zhang, Y. Tang, and F. Qian, “Monocular depth estimation based on deep learning: An overview,” *Science China Technological Sciences*, vol. 63, no. 9, pp. 1612–1627, 2020.
- [20] V. Sitzmann, S. Diamond, Y. Peng, X. Dun, S. Boyd, W. Heidrich, F. Heide, and G. Wetzstein, “End-to-end optimization of optics and image processing for achromatic extended depth of field and super-resolution imaging,” *ACM Transactions on Graphics (TOG)*, vol. 37, no. 4, pp. 1–13, 2018.
- [21] H. Arguello, J. Bacca, H. Kariyawasam, E. Vargas, M. Marquez, R. Hettiarachchi, H. Garcia, K. Herath, U. Haputhanthri, B. S. Ahluwalia *et al.*, “Deep optical coding design in computational imaging: a data-driven framework,” *IEEE Signal Processing Magazine*, vol. 40, no. 2, pp. 75–88, 2023.
- [22] J. Chang and G. Wetzstein, “Deep optics for monocular depth estimation and 3d object detection,” in *Proceedings of the IEEE/CVF International Conference on Computer Vision*, 2019, pp. 10 193–10 202.
- [23] Y. Wu, V. Boominathan, H. Chen, A. Sankaranarayanan, and A. Veeraraghavan, “Phasecam3d—learning phase masks for passive single view depth estimation,” in *2019 IEEE International Conference on Computational Photography (ICCP)*. IEEE, 2019, pp. 1–12.
- [24] S.-H. Baek, H. Ikoma, D. S. Jeon, Y. Li, W. Heidrich, G. Wetzstein, and M. H. Kim, “Single-shot hyperspectral-depth imaging with learned diffractive optics,” in *Proceedings of the IEEE/CVF International Conference on Computer Vision*, 2021, pp. 2651–2660.
- [25] E. Vargas, J. N. Martel, G. Wetzstein, and H. Arguello, “Time-multiplexed coded aperture imaging: Learned coded aperture and pixel exposures for compressive imaging systems,” in *Proceedings of the IEEE/CVF International Conference on Computer Vision*, 2021, pp. 2692–2702.
- [26] Y. Wang, F. Liu, Z. Wang, G. Hou, Z. Sun, and T. Tan, “End-to-end view synthesis for light field imaging with pseudo 4dcnn,” in *Proceedings of the European Conference on Computer Vision (ECCV)*, 2018, pp. 333–348.
- [27] H. Ikoma, C. M. Nguyen, C. A. Metzler, Y. Peng, and G. Wetzstein, “Depth from defocus with learned optics for imaging and occlusion-aware depth estimation,” in *2021 IEEE International Conference on Computational Photography (ICCP)*. IEEE, 2021, pp. 1–12.
- [28] Y. D. Salman, K. R. Ku-Mahamud, and E. Kamioka, “Distance measurement for self-driving cars using stereo camera,” in *International Conference on Computing and Informatics*, vol. 1, no. 105, 2017, pp. 235–242.
- [29] M. Okutomi and T. Kanade, “A multiple-baseline stereo,” in *CVPR*, vol. 93, 1991, pp. 63–69.
- [30] F. Khan, S. Salahuddin, and H. Javidnia, “Deep learning-based monocular depth estimation methods—a state-of-the-art review,” *Sensors*, vol. 20, no. 8, p. 2272, 2020.
- [31] S. K. Nayar, M. Watanabe, and M. Noguchi, “Real-time focus range sensor,” *IEEE Transactions on Pattern Analysis and Machine Intelligence*, vol. 18, no. 12, pp. 1186–1198, 1996.
- [32] S. Hiura and T. Matsuyama, “Depth measurement by the

- multi-focus camera,” in *Proceedings. 1998 IEEE Computer Society Conference on Computer Vision and Pattern Recognition (Cat. No. 98CB36231)*. IEEE, 1998, pp. 953–959.
- [33] Y. Takeda, “Coded aperture stereo for extension of depth of field and refocusing,” in *Int. Conf. on Computer Vision Theory and Applications, 2012*, 2012, pp. 103–111.
- [34] Y. Amari and E. H. Adelson, “Single-eye range estimation by using displaced apertures with color filters,” in *Proceedings of the 1992 International Conference on Industrial Electronics, Control, Instrumentation, and Automation*. IEEE, 1992, pp. 1588–1592.
- [35] A. Chakrabarti and T. Zickler, “Depth and deblurring from a spectrally-varying depth-of-field,” in *Computer Vision—ECCV 2012: 12th European Conference on Computer Vision, Florence, Italy, October 7-13, 2012, Proceedings, Part V 12*. Springer, 2012, pp. 648–661.
- [36] V. Paramonov, I. Panchenko, V. Bucha, A. Drogolyub, and S. Zagoruyko, “Depth camera based on color-coded aperture,” in *Proceedings of the IEEE Conference on Computer Vision and Pattern Recognition Workshops*, 2016, pp. 1–9.
- [37] H. Arguello, S. Pinilla, Y. Peng, H. Ikoma, J. Bacca, and G. Wetzstein, “Shift-variant color-coded diffractive spectral imaging system,” *Optica*, vol. 8, no. 11, pp. 1424–1434, 2021.
- [38] H. Haim, S. Elmaleh, R. Giryas, A. M. Bronstein, and E. Marom, “Depth estimation from a single image using deep learned phase coded mask,” *IEEE Transactions on Computational Imaging*, vol. 4, no. 3, pp. 298–310, 2018.
- [39] R. Hecht-Nielsen, “Theory of the backpropagation neural network,” in *Neural networks for perception*. Elsevier, 1992, pp. 65–93.
- [40] J. Bacca, T. Gelvez-Barrera, and H. Arguello, “Deep coded aperture design: An end-to-end approach for computational imaging tasks,” *IEEE Transactions on Computational Imaging*, vol. 7, pp. 1148–1160, 2021.
- [41] H. Arguello and G. R. Arce, “Colored coded aperture design by concentration of measure in compressive spectral imaging,” *IEEE Transactions on Image Processing*, vol. 23, no. 4, pp. 1896–1908, 2014.
- [42] J. W. Goodman, *Introduction to Fourier optics*. Roberts and Company Publishers, 2005.
- [43] S. W. Hasinoff and K. N. Kutulakos, “A layer-based restoration framework for variable-aperture photography,” in *2007 IEEE 11th International Conference on Computer Vision*. IEEE, 2007, pp. 1–8.
- [44] I. Sobel and G. Feldman, “A 3x3 isotropic gradient operator for image processing,” *a talk at the Stanford Artificial Project in*, pp. 271–272, 1968.
- [45] J. Hu, M. Ozay, Y. Zhang, and T. Okatani, “Revisiting single image depth estimation: Toward higher resolution maps with accurate object boundaries,” in *2019 IEEE Winter Conference on Applications of Computer Vision (WACV)*. IEEE, 2019, pp. 1043–1051.
- [46] R. Girshick, “Fast r-cnn,” in *Proceedings of the IEEE international conference on computer vision*, 2015, pp. 1440–1448.
- [47] I. Goodfellow, Y. Bengio, and A. Courville, *Deep learning*. MIT press, 2016.
- [48] A. Paszke, S. Gross, F. Massa, A. Lerer, J. Bradbury, G. Chanan, T. Killeen, Z. Lin, N. Gimelshein, L. Antiga *et al.*, “Pytorch: An imperative style, high-performance deep learning library,” *Advances in neural information processing systems*, vol. 32, pp. 8026–8037, 2019.
- [49] P. K. Nathan Silberman, Derek Hoiem and R. Fergus, “Indoor segmentation and support inference from rgb-d images,” in *ECCV*, 2012.
- [50] Y. Zhao, L.-M. Po, Q. Yan, W. Liu, and T. Lin, “Hierarchical regression network for spectral reconstruction from rgb images,” in *Proceedings of the IEEE/CVF Conference on Computer Vision and Pattern Recognition Workshops*, 2020, pp. 422–423.
- [51] J. M. Bioucas-Dias and G. Valadao, “Phase unwrapping via graph cuts,” *IEEE Transactions on Image processing*, vol. 16, no. 3, pp. 698–709, 2007.
- [52] R. Ranftl, A. Bochkovskiy, and V. Koltun, “Vision transformers for dense prediction,” in *Proceedings of the IEEE/CVF International Conference on Computer Vision*, 2021, pp. 12 179–12 188.
- [53] H. Fu, M. Gong, C. Wang, K. Batmanghelich, and D. Tao, “Deep ordinal regression network for monocular depth estimation,” in *Proceedings of the IEEE conference on computer vision and pattern recognition*, 2018, pp. 2002–2011.
- [54] D. Xu, E. Ricci, W. Ouyang, X. Wang, and N. Sebe, “Multi-scale continuous crfs as sequential deep networks for monocular depth estimation,” in *Proceedings of the IEEE conference on computer vision and pattern recognition*, 2017, pp. 5354–5362.
- [55] J. Li, R. Klein, and A. Yao, “A two-streamed network for estimating fine-scaled depth maps from single rgb images,” in *Proceedings of the IEEE International Conference on Computer Vision*, 2017, pp. 3372–3380.
- [56] A. Saxena, M. Sun, and A. Y. Ng, “Learning 3-d scene structure from a single still image,” in *2007 IEEE 11th international conference on computer vision*. IEEE, 2007, pp. 1–8.
- [57] I. Laina, C. Rupprecht, V. Belagiannis, F. Tombari, and N. Navab, “Deeper depth prediction with fully convolutional residual networks,” in *2016 Fourth international conference on 3D vision (3DV)*. IEEE, 2016, pp. 239–248.
- [58] W. Yin, Y. Liu, C. Shen, and Y. Yan, “Enforcing geometric constraints of virtual normal for depth prediction,” in *Proceedings of the IEEE/CVF International Conference on Computer Vision*, 2019, pp. 5684–5693.
- [59] J. H. Lee, M.-K. Han, D. W. Ko, and I. H. Suh, “From big to small: Multi-scale local planar guidance for monocular depth estimation,” *arXiv preprint arXiv:1907.10326*, 2019.
- [60] M. Song, S. Lim, and W. Kim, “Monocular depth estimation using laplacian pyramid-based depth residuals,” *IEEE transactions on circuits and systems for video technology*, vol. 31, no. 11, pp. 4381–4393, 2021.
- [61] S. F. Bhat, I. Alhashim, and P. Wonka, “Adabins: Depth estimation using adaptive bins,” in *Proceedings of the IEEE/CVF Conference on Computer Vision and Pattern*

Recognition, 2021, pp. 4009–4018.

- [62] “Fujifilm fujichrome velvia 50 professional rvp 50 color transparency film (35mm roll film, 36 exposures).” [Online]. Available: https://www.bhphotovideo.com/c/product/512063-USA/Fujifilm_15757464_RVP_135_36_Fujichrome_Velvia.html